Does the Oxygen Evolution Reaction Follow the classical OH*, O*, OOH* Path on Single Atom Catalysts?

Ilaria Barlocco, Luis A. Cipriano, Giovanni Di Liberto, Gianfranco Pacchioni
Dipartimento di Scienza dei Materiali, Università di Milano - Bicocca,
via R. Cozzi 55, 20125 Milano, Italy
gianfranco.pacchioni@unimib.it

07/09/2022

Abstract

The Oxygen Evolution Reaction (OER) is a key part of water splitting. On metal and oxide surfaces it usually occurs *via* formation of three intermediates, M(OH), M(O), and M(OOH) (also referred to as OH*, O*, and OOH* species where * indicates a surface site). The last step consists of O_2 release. So far, it has been generally assumed that the same path occurs on single atom catalysts (SACs). However, the chemistry of SACs may differ substantially from that of extended surfaces and is reminiscent of that of coordination compounds. This raises the question of whether on SACs the OER follows the classical mechanism or not. Using a DFT approach, we studied a set of 30 SACs made by ten metal atoms (Sc, Ti, V, Cr, Mn, Fe, Co, Ni, Pd and Pt) anchored on three widely used 2D carbon-based materials, graphene, nitrogen-doped graphene and carbon nitride. In none of the cases examined the most favourable reaction path is the conventional one. In fact, in all cases other intermediates with higher stabilities form: $M(OH)_2$, M(O)(OH), $M(O)_2$, and $M(O_2)$ (OH* OH*, O* OH*, O* O*, O_2* according to standard nomenclature). Therefore, the common assumption that on SACs the OER proceeds via formation of OH*, O*, and OOH* intermediates is not verified. Predictions of new catalysts based on the screening of large number of potential structures can lead to completely incorrect conclusions if these additional intermediates are not taken into consideration.

Keywords: OER, SACs, C_3N_4, N-doped graphene, DFT

1. Introduction

The reaction of water splitting is a subject of intense research since a long time.[1–4] The process is endergonic and converts water molecules into molecular oxygen and hydrogen, a key molecule for the energy transition. The process $2H_2O \rightarrow 2H_2 + O_2$ has a thermodynamic cost of 4.92 eV, and in reality is even larger due to the overpotentials of both the cathodic and anodic semi-reactions.[5] Among the best catalysts is Platinum, which however poses problems of costs and availability of critical raw materials. Not surprisingly, the efforts are concentrated on the search of novel catalysts able to promote the reaction with low extra energy costs and using abundant elements or, as an alternative, very low amounts of noble metals. This explains the high interest on Single Atom Catalysts (SAC), a relatively new frontier in catalysis, although the concept of single site is probably more appropriate.[6,7]

SACs consist of isolated metal atoms stably anchored on a support. They can have good thermal stability and high activity, and sometimes their behaviour can be rationalized in terms of coordination chemistry. In this respect, the chemistry of SACs can be very different from that of an extended metal surface.[8]

The Oxygen Evolution Reaction (OER) takes place in the oxidation semi-reaction of water splitting. On metal catalysts the process usually occurs *via* formation of three chemical intermediates, each one releasing one electron (* indicates the adsorption site):[9–11]

$$H_2O + * \rightarrow OH* + H^+ + e^- \quad \text{Eq. 1}$$

$$OH* \rightarrow O* + H^+ + e^- \quad \text{Eq. 2}$$

$$H_2O + O* \rightarrow OOH* + H^+ + e^- \quad \text{Eq. 3}$$

In the last step a fourth electron is released together with the free O_2 molecule:

$$OOH* \rightarrow O_{2\,(g)} + * + H^+ + e^- \quad \text{Eq. 4}$$

The OER on a metal or oxide surface can be modelled with electronic structure methods by adopting a relatively simple yet efficient approach proposed by Nørskov and co-workers.[9,12–14] According to this approach the Gibbs energy profile of the reaction can be generated by evaluating the stability of each intermediate and neglecting any other reaction barrier. Although simplified, the model turned out to be extremely successful and insightful.[15–18]

The formation of the "classical" OH*, O*, and OOH* intermediates (Eq. 1-4) is commonly assumed also when working with SACs, and the conceptual model adopted for extended surfaces is transferred to SACs without changes. However, SACs are analogues of coordination compounds,[19] and as such they can display a very different chemistry compared to extended surfaces. In particular, new chemical species can be stabilized on isolated transition metal (TM) atoms, leading to other intermediates beside the classical ones.[20] This opens the general and relevant question whether on SACs the OER follows the classical OH*, O*, OOH* path or not.

To answer this question, we performed quantum chemical calculations on a series of SACs. Our work is motivated by two recent observations done in our group. The first one is that in the study of the Hydrogen Evolution Reaction (HER), the other semi-reaction in water splitting, it is usually assumed that on SACs only one intermediate plays an important role, a single H atom adsorbed on the catalytic center M (MH). However, we demonstrated that while this assumption is correct for metal surfaces,[21] it is no longer valid on SACs where stable dihydride or dihydrogen intermediates (HMH) can form, changing the kinetics of the process.[22] The second observation is somewhat similar to the first one, but is related to the OER. Also in this case, we have shown recently that before O_2 is released from the catalyst, see Eq. 4, stable superoxo and peroxo complexes can form on SACs, at variance with extended surfaces.[23] This shows that on SACs the path leading to water oxidation can be more complex than described by Eq.s 1-4. Notice also that the formation of different chemical intermediates is of broader interest. They have been observed in other materials such as ABO_3 perovskite oxides and RuO_2 to name a few.[24–29]

In this work we considered three different and widely adopted carbon-based supports,[30–35] and we anchored a set of ten metal atoms (Sc, Ti, V, Cr, Mn, Fe, Co, Ni, Pd and Pt) on a C double vacancy on graphene (DV-Gr), on nitrogen-doped graphene (4N-Gr), and on carbon nitride (C_3N_4), Figure 1, for a total of 30 structures.

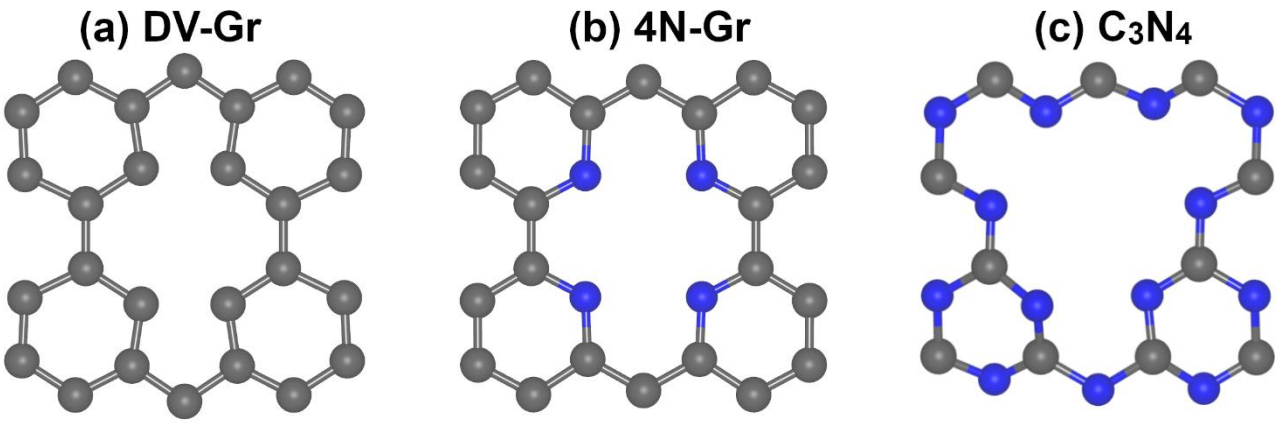

Figure 1: The supports investigated in this work: a) C divacancy on graphene (DV-Gr), b) Nitrogen-doped graphene (4N-Gr) and c) carbon nitride (C_3N_4). The metal atoms are stabilized in the cavities present in the structures.

The family of intermediates examined includes, besides the three classical OH*, O*, and OOH* species, eight different complexes, Figure 2. Some of these complexes are simply combination of the "basic" intermediates, as metal centers can bind simultaneously two OH groups, one OH and one O, or even two O atoms; furthermore, the complexes can assume a *sin* or an *anti*-configuration, depending on the adsorption on the same or on the opposite sites of the 2D carbon structure, see Figure 2. These additional intermediates are not unprecedented. Some of them have been observed in selected systems,[20],[36–39] but the importance and generality of their formation in the OER has not been recognized so far. Furthermore, no systematic study of the non-conventional intermediates in OER on SACs has been reported.

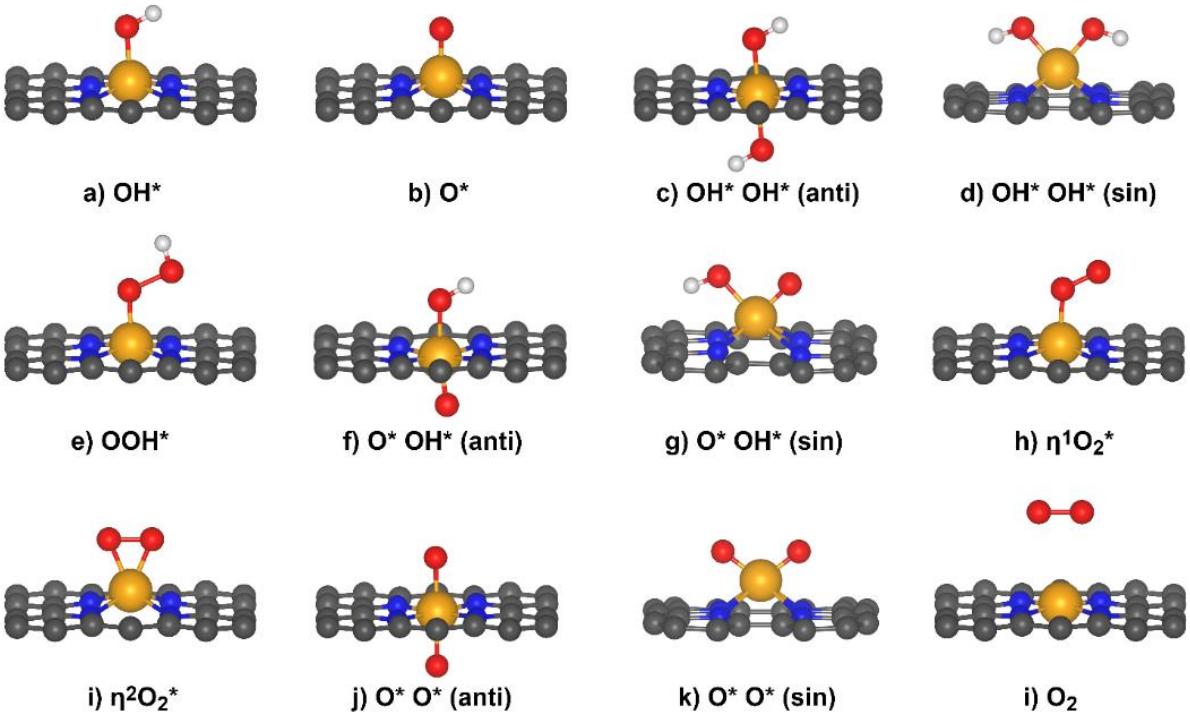

Figure 2: Possible OER intermediates on SACs embedded in 2D carbon nanostructures (N-doped graphene, 4N-Gr, is reported as an example). Similar structures have been considered on the other supports (DV-Gr and C_3N_4, see also Figure 1).

Our results indicate that in none of the 30 SACs considered the most favourable reaction path is characterized by the three classical intermediates, since in all cases at least one, and often more than one, unconventional stable intermediate forms, thus changing the reaction profile and introducing new barriers in the process. This conclusion is relevant as it indicates that the predicted activity of a new potential SAC in OER based on DFT needs to consider more complex paths than usually assumed. In this respect, the numerous reports of screening of OER catalytic activity of large number of SACs[40–42] based on the classical intermediates should be considered cautiously, as the general assumption that the same mechanism governs the reaction on metal surfaces or on SACs is not verified.

It is also worth mentioning that the thermodynamic approaches usually adopted in the theoretical study of OER contain several approximations. For instance, solvation, *p*H and other effects

are not included, limiting the quantitative nature of the results.[43–48] This is also true here. However, the purpose of this work is not to provide yet another prediction of good or bad catalyst in OER, but rather to provide a general message: when the OER occurs on SACs other reaction intermediates may form, usually not considered, altering the "classical" mechanism of the reaction. Of course, this means an increased complexity for the modelling of these class of reactions, but the oversimplification of the problem can lead to completely incorrect conclusions.

2 Computational Details

Spin polarized DFT calculations were performed with the VASP[49–51] code using the generalized gradient approximation, as implemented in the Perdew–Burke–Ernzerhof (PBE) functional.[52] Dispersion forces have been included according to the Grimme's D3 parametrization.[53] The following valence electrons were treated explicitly: H (1s), C (2s,2p), N (2s, 2p), O (2s, 2p), Sc (3s, 3p, 4s, 3d), Ti (3s, 3p, 4s, 3d), V (3s, 3p, 4s, 3d), Cr (3p, 4s, 3d), Mn (3p, 4s, 3d), Fe (4s, 3d), Co (4s, 3d), Ni (4s, 3d), Pd (5s, 4d), and Pt (6s, 5d). They have been expanded on a set of plane waves with a kinetic energy cutoff of 400 eV, whereas the core electrons were treated with the projector augmented wave approach (PAW).[54,55] The threshold criteria for electronic and ionic loops were set to 10^{-5} eV and 10^{-3} eV/Å, respectively. A 5×5×1 Monkhorst−Pack k-point grid[56] was used to sample the reciprocal space for graphene and N-doped graphene, and reduced to 1×2×1 for C_3N_4 because of the cell dimension.

A 4×4×1 supercell of graphene was created considering the pristine graphene lattice parameters ($a = b = 2.468$ Å, $\gamma = 120^{o}$) and adding a vacuum layer of 15 Å to avoid spurious effects due to interaction between periodic replica of the system along the non-periodic direction. The supercell was fully optimized (lattice parameters $a = b = 9.870$ Å, $\gamma = 120^{o}$).[57,58] Then, we created a carbon divacancy (DV-Gr) and relaxed the atomic coordinates. The metal single atoms were anchored in the resulting cavity in the graphene layer, Figure 1a. The Nitrogen-doped graphene model

was generated by creating a C divacancy replacing four C with N atoms and relaxing the atomic coordinates. The metal atoms were embedded in the cavity, Figure 1b. Last, we considered a corrugated C_3N_4 layer characterized by heptazine pores and we optimized the lattice parameters (a = 13.846 Å, b = 6.923 Å, γ = 120º).[59,60] The metal atoms were adsorbed inside the pore Figure 1c.

The binding energies (ΔE) of each intermediate were calculated using the optimized structures and the free atoms and catalysts as references. The Gibbs energies were evaluated by adding zero-point energy correction and entropy terms. The first were calculated in a harmonic fashion (details can be found in Section S1 and in Ref. [23]). Entropies of gases were taken from the international tables, and the entropy of solid-state species were considered equal to zero,[23] see section S2.[61] Given the specific purpose of this study, which is not to provide highly accurate numbers but rather to compare the stability of species with a similar framework, the adopted approximation can be considered acceptable.

3 Results and Discussion

Table 1 reports the calculated binding energies, selected bond distances and the magnetization of the TM atoms stabilized in the three supports described above (Figure 1). In all cases, the metal atoms are strongly bound to the supporting layer, Table 1, although with sizeable changes in stability (see Figure S1 for the optimized structure of every SAC).

Table 1: Binding energies, bond distances and atomic magnetization of TM atoms incorporated in a divacancy of graphene (DV-Gr), N-doped graphene (4N-Gr) and C_3N_4.

Catalyst	E_B / eV	R(M---N) / Å	R(M---C) / Å	Magnetization /μ_B
Sc@DV-Gr	-6.30	-	2.18	0.00
Ti@DV-Gr	-8.18	-	2.06	0.00
V@DV-Gr	-7.53	-	2.01	0.78
Cr@DV-Gr	-6.26	-	2.00	2.17
Mn@DV-Gr	-6.12	-	1.99	2.98
Fe@DV-Gr	-6.72	-	1.96	2.36
Co@DV-Gr	-7.05	-	1.94	0.92
Ni@DV-Gr	-6.98	-	1.89	0.00

Pd@DV-Gr	-5.38	-	2.02	0.00
Pt@DV-Gr	-7.83	-	1.96	0.00
Sc@4N-Gr	-8.43	2.08	-	0.00
Ti@4N-Gr	-8.50	1.97-2.08	-	0.88
V@4N-Gr	-7.86	1.98	-	2.09
Cr@4N-Gr	-7.20	1.95	-	3.25
Mn@4N-Gr	-6.80	1.92	-	2.94
Fe@4N-Gr	-7.39	1.90	-	1.86
Co@4N-Gr	-7.79	1.89	-	0.76
Ni@4N-Gr	-7.78	1.89	-	0.00
Pd@4N-Gr	-6.03	1.95	-	0.00
Pt@4N-Gr	-7.99	1.96	-	0.00
Sc@C_3N_4	-6.69	2.27-2.37	-	0.26
Ti@C_3N_4	-6.28	2.26-2.42	-	1.27
V@C_3N_4	-5.05	2.14-2.23	-	2.45
Cr@C_3N_4	-3.57	2.14-2.51	-	3.71
Mn@C_3N_4	-3.36	2.25-2.56	-	4.28
Fe@C_3N_4	-3.45	2.13-2.45	-	3.27
Co@C_3N_4	-3.34	1.99-2.26	-	1.93
Ni@C_3N_4	-3.47	1.95-1.97	-	0.92
Pd@C_3N_4	-2.24	2.14-2.26	-	0.00
Pt@C_3N_4	-2.79	2.05-2.16	-	0.00

In particular, one goes from -8.5 eV of Ti@4N-Gr to -2.24 eV of Pd@C_3N_4. Clearly, these differences are expected to reflect in a different stability and sintering resistance of the complexes. This is particularly relevant for C_3N_4, where the metal atoms can bind to three stable minima separated by about 0.3 eV within the heptazine pore. In each case, the global minimum was always considered. The existence of several local minima with similar energies suggests mobility and low thermal stability, a problem which is of paramount importance for the design of a new catalyst. Nevertheless, this aspect is minor relevance for the present study where the aim is to show the possible formation of various intermediates.

We now consider the formation and stability of reaction intermediates. The conventional path starts with the formation of OH* from the reaction between the catalyst with a water molecule, Figure 2a, with release of one proton and one electron (Eq. 1). Upon release of a second electron O* adsorbed species can form (Eq. 2), Figure 2b. In the next step, if the system releases a third electron, the OOH* complex can form from the interaction of O* with a water molecule (Eq. 3), Figure 2e. Finally, OOH*,

upon release of the fourth and last electron, leads to the formation of a O_2 molecule that desorbs in the gas-phase, regenerating the catalyst and closing the cycle.

However, the formation of other complexes is also possible. After formation of OH*, Eq. 1, the metal site can bind a second hydroxyl group, leading to a complex with two bound OH groups, OH* OH*, Figures 2c and 2d:

$$2H_2O + * \rightarrow OH^* OH^* + 2H^+ + 2e^- \quad \text{Eq. 5}$$

The formation of OH* OH* implies the release of two electrons, and therefore this intermediate can form in alternative to the classical O* species, Eq. 2.[20] Recently, Zhong and Li showed by means of electronic structure calculations on Fe and Co atoms embedded in carbon-based matrices that the OH* OH* complex is more stable than the O* one.[20] Of course, the formation of the unconventional OH* OH* intermediate does not exclude that in the next step the reaction proceeds with the classical path, since the OOH* species can form starting from the OH* OH* complex according to Eq. 6:

$$OH^* OH^* \rightarrow OOH^* + H^+ + e^- \quad \text{Eq. 6}$$

However, once the O* or OH* OH* intermediates are formed, the reaction can proceed via formation of other species beside OOH*. For instance, the OH* OH* complex can release a proton and an electron forming the OH* O* [38] species, where both an O atom and an OH group are bound to the TM, Figures 2f and 2g and Eq. 7:

$$OH^* OH^* \rightarrow OH^* O^* + H^+ + e^- \quad \text{Eq. 7}$$

The formation of this complex is competitive with the OOH* species (in both cases the release of three electrons is involved). The simultaneous presence of OH* and O* species has been postulated in the study of the ORR reaction over Pt_3M alloys.[38]

No matter if the reaction proceeds via formation of the "new" OH* O* species or the "classical" OOH* one, both can lead to the formation of peroxo or superoxo O_2* complexes, Figures 2h and 2i, according to Eq.s 8 and 9:

$$OH^* O^* \rightarrow O_2^* + H^+ + e^- \quad \text{Eq. 8}$$

$$OOH^* \rightarrow O_2^* + H^+ + e^- \quad \text{Eq. 9}$$

Recently, we showed that stable superoxo and peroxo complexes can form on SACs, introducing an additional step before the release of the O_2 molecule to the gas-phase.[23] This is not surprising considering that these are well known species in coordination chemistry. This has important implications for the kinetics of the process since Eq. 4 is no longer valid and must be replaced by the following step:

$$O_2^* \rightarrow O_{2\,(g)} + * \quad \text{Eq. 10}$$

As an alternative, the OH* O* or the OOH* complexes can form a competitive species where two separate O* atoms are adsorbed on the same metal site,[36] O* O*, see Figures 2j and 2k and Eq. 11 and Eq. 12:

$$OH^* O^* \rightarrow O^* O^* + H^+ + e^- \quad \text{Eq. 11}$$

$$OOH^* \rightarrow O^* O^* + H^+ + e^- \quad \text{Eq. 12}$$

The complexity of the picture increases further if one considers that for each of the OH* OH*, O* O*, and OH* O* complexes two different conformers may exist on a SAC consisting of a metal atom embedded in a 2D material. In fact, the two O-related ligands can bind on the same side (*sin*), or on opposite sides (*anti*) of the plane containing the metal atom, see Figures 2c and 2d, 2f and 2g, 2j and 2k.

The series of possible reaction paths and their interconnections are summarized in Scheme 1. The usually assumed path is marked in bold, but the richness of the chemistry of the systems

considered opens a number of possible alternative paths. It is obvious that only if the mechanism of the reaction is correctly identified reliable predictions about the activity of a catalyst can be made.

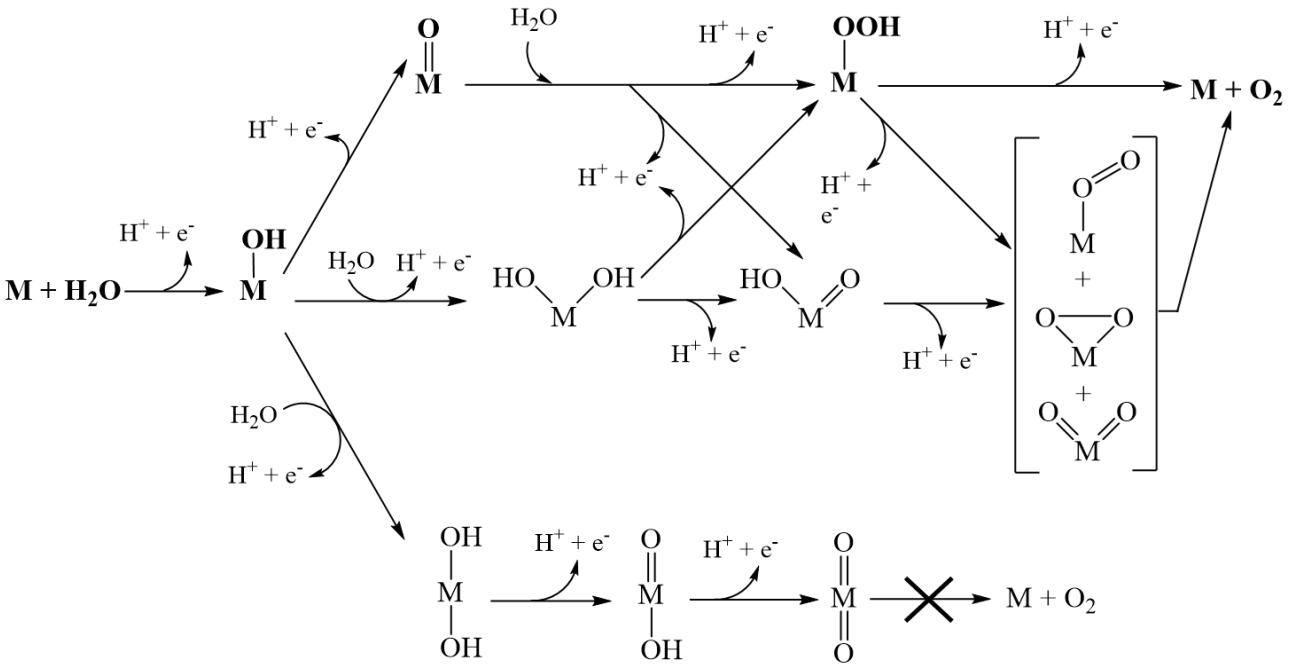

Scheme 1: Oxygen evolution reaction (OER) scheme were all the possible pathways are showed including the formation of all possible "classical" (in bold) and "unconventional" intermediates. The following correspondence of notations is adopted: OH* (M-OH); O* (M=O); OOH* (M-OOH); OH* OH* ($M(OH)_2$); OH* O* (M(OH)(O)); O_2* ($M\text{-}O_2$); O* O* (O=M=O). The path that implies the formation of the *anti* O* O* complex (O=M=O) cannot lead to the formation and the release of molecular oxygen unless very high barriers are overcome.

In this respect, it is worth mentioning that reaction paths that imply the formation of *sin*- and *anti*-conformers are completely separated, as the interconversion of one isomer into the other is prevented by the existence of the extended layer around the metal center. In other words, a *sin* intermediate cannot directly convert into an *anti*-one. This means that the formation of the *anti*- form of the O* O* intermediate cannot lead to the release of O_2 unless very high barriers are overcome.

From this point of view, the formation of this complex can be considered as a sort of catalyst poisoning (Scheme 1).

Once we have defined all possible reaction paths, we evaluated the stability of each intermediate and we determined the most-likely path[9] based on the Gibbs energies profile, assuming that a working voltage of 1.23 V is applied.

Interestingly, the Gibbs energy profiles indicate that in none of the 30 SACs considered the OER follows the classical OH*, O*, OOH* path, since at least one unconventional species is found to be more stable. The case of single atoms anchored to C_3N_4 is paradigmatic. The unconventional intermediates are more stable than the classical ones for all ten TM atoms considered. For instance, on average, the OH* OH* non-classical intermediate shows a Gibbs energy 0.9 eV lower than the classical O* species. Considering the following step, the new OH* O* species is, in average, 2.0 eV more stable than the classical OOH* one. This is a very large energy difference, and on these systems the formation of the conventional OOH* intermediate becomes very unlikely (not to say impossible). The same is true for all systems considered, as it is shown in Figures S2-S4 and Tables S3-S5 of the Supporting Information. This trend will be further discussed in the next Section where selected examples will be examined in more detail.

4 Selected examples of mechanisms of OER on SACs

In the previous Section we have shown that the OER can follow more complex paths than usually assumed, and that several intermediates can form with higher stability than the classical ones. Since a detailed analysis of the 30 cases of SACs considered in this work would be redundant, we limit ourselves to the discussion of few selected cases of reactivity that can be considered representative of the various paths that can lead to the conversion of H_2O in O_2.

We start by considering the Gibbs energy profile of a Ti atom embedded in a graphene matrix, Ti@DV-Gr, Figure 3a. Here the process follows the standard path, with formation of OH* (step 1), O* (step 2), and OOH* (step 3). Notice that on Ti@DV-Gr the OH* OH* complex can form, but its energy is higher than that of the O* complex, Figure 3a. The deviation from the standard path occurs when one considers the fourth and last step. In fact, instead of forming directly O_2, Eq. 4, the reaction proceeds with formation of a stable peroxo complex, η^2-O_2*. This species is about 0.7 eV below the OOH* complex, Figure 3a. The O* O* and the superoxo η^1-O_2* species can also form on Ti@DV-Gr but with slightly higher energies, Figure 3a. As discussed in our recent study, the formation of the peroxo intermediate has important consequences on the kinetics. Here, for instance, the high stability of this complex results in a considerable barrier for O_2 release, Figure 3a.

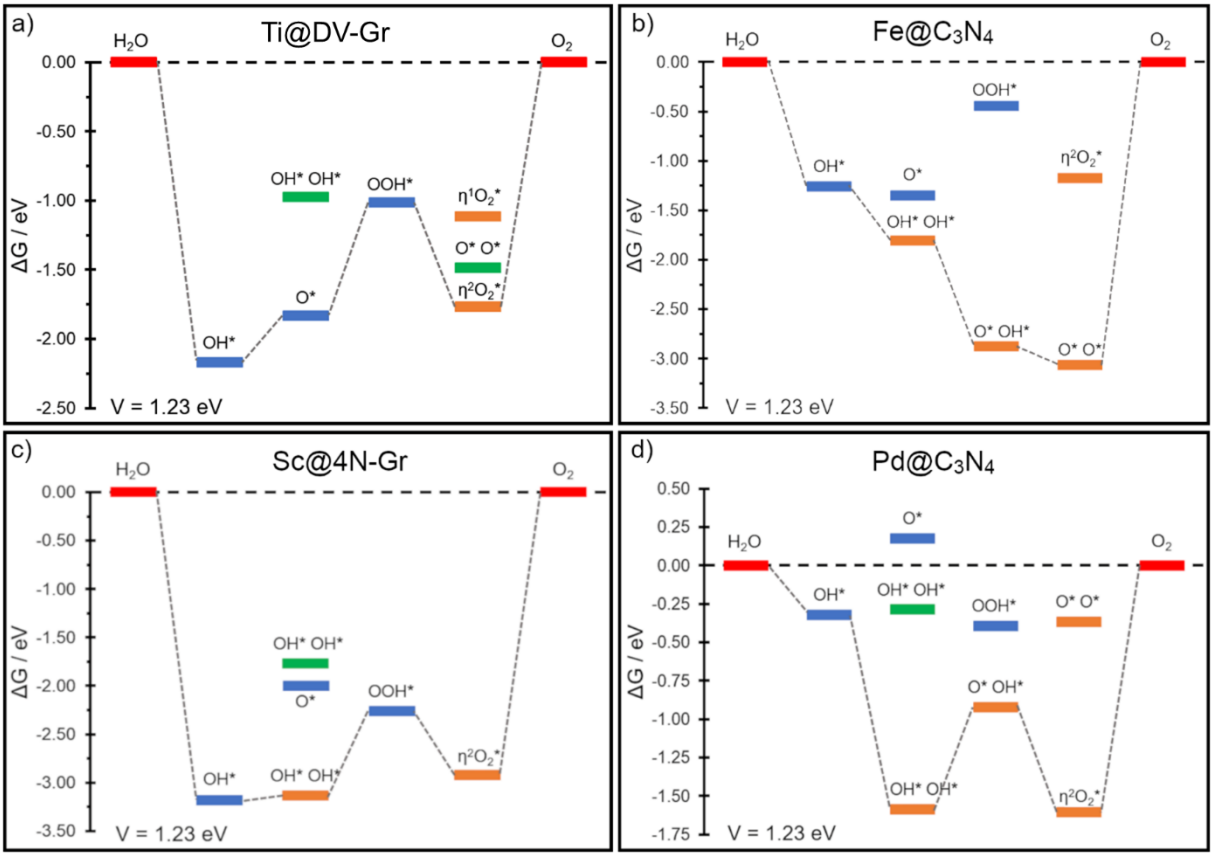

Figure 3: Gibbs energy profile of: a) Ti@DV-Gr, here only one unconventional intermediate forms, η^2-O_2*; b) Fe@C_3N_4, here the entire pathway is characterised by the formation of unconventional intermediates; c) Sc@4N-Gr, here two intermediates are "classical" and two are unconventional; (d) Pd@C_3N_4, here the classical (blue) and the unconventional (orange) paths lead to completely different predictions about the reactivity of the SAC. The conventional intermediates

are represented in blue, the unconventional *sin* and *anti* are in orange and green, respectively. The Gibbs energy profile is reported at V = 1.23 eV and the experimental reference energy of O_2 molecule was considered.

If the case of Ti@DV-Gr represents an example of OER that, apart from the last step, follows the classical mechanism, Fe@C_3N_4 is a catalyst where, apart from the first step, all the rest of the reaction follows a completely different path due to the formation of very stable unconventional intermediates. The formation of the OH* complex (step 1) is followed by the formation of the OH* OH* complex, Figure 3b, which is about 0.6 eV more stable than the classical O* intermediate. The release of the third electron, instead of leading to OOH*, results in the formation of a very stable O* OH* intermediate which is about 2.5 eV below the classical OOH* species, Figure 3b. The high reactivity of Fe@C_3N_4 leads to a very stable O* O* intermediate before the release of O_2, Figure 3b. The consequence is that O_2 formation implies a huge barrier, >3 eV, making this system totally unsuitable to catalyse the OER. Notice that completely different conclusions would be reached by looking only at the classical reaction profile, as the highest barrier (of the order of 1 eV) would be that to convert O* into OOH*, Figure 3b.

In other SACs the reaction profile can be considered as a mix of classical and unconventional paths. In Sc@4N-Gr, after the formation of the OH* complex (step 1), in step 2 the OH* OH* species forms, as this is about 1 eV more stable than the classical O* complex, Figure 3c. In step 3, however, the OH* OH* species converts into the classical OOH* intermediate, as no other stable species can form in this step. Next, a stable η^2-O_2* peroxo complex forms, and from this O_2 is released, again with a huge energy barrier, Figure 3c. For this hypothetical SAC, two intermediates are of the classical type, and the other two are unconventional.

To show how the choice to consider only the traditional path compared to the one in which new intermediates can form affects the overall conclusions on the activity of the catalyst, let's discuss the case of Pd@C_3N_4, Figure 3d. Here the classical path, OH*, O*, OOH* and O_2 occurs with relatively small free energy changes, always below 0.3 eV, Figure 3d. However, on this SAC some

complexes can have completely different stabilities, such as the *sin*-OH* OH* species and the η^2-O_2* peroxo complex, Figure 3d. These complexes are about 1.5 eV more stable than the corresponding classical intermediates, introducing reaction barriers that strongly reduce the expected catalytic activity. Thus, while according to the standard model Pd@C_3N_4 is an excellent catalyst, following the new more complex path the same system is predicted to be rather inactive.

In the last two cases we discuss the role played by the possible formation of *sin* and *anti* isomers when two O-related ligands bind to the same metal center. The first case is that of Pt@C_3N_4, Figure 4a. Here, after the first step, OH* formation, the SAC forms a OH* OH* complex that competes in stability with the classical O* one. However, while the *sin*-OH* OH* complex is about 0.5 eV more stable than the O* one, the *anti*-OH* OH* complex is less stable than O* by about the same amount, 0.5 eV, Figure 4b. On this SAC, also step 3 is unconventional, but here both the *sin* and the *anti* isomers of the O* OH* complex are more favorable than the classical OOH* species, Figure 4a. As for many other SACs considered in this study, the last step, O_2 release, is preceded by the formation of a η^2-O_2* peroxo complex, Figure 4a. Notice that on Pt@C_3N_4 the *sin* isomers are always preferred over the *anti* ones.

This is different from what found for Mn@4N-Gr, see Figure 4b. Here the reaction follows the classical path for the first two steps, OH* and O*, but then the formation of the O* OH* complex is much more favorable than the classical OOH* intermediate, Figure 4b. This is true for both the *sin* and the *anti* O* OH* isomers, but at variance with the Pt@C_3N_4 case, the *anti* species is definitely preferred and is followed by the formation of the *anti*-O* O* complex, Figure 4b and Figure 2j. The *anti* O* O* intermediate represents a dead-end for the reaction as it will be impossible to recombine the two O* atoms bound on the opposite sites of the graphene layer to form the O_2 molecule, see also Scheme 1.

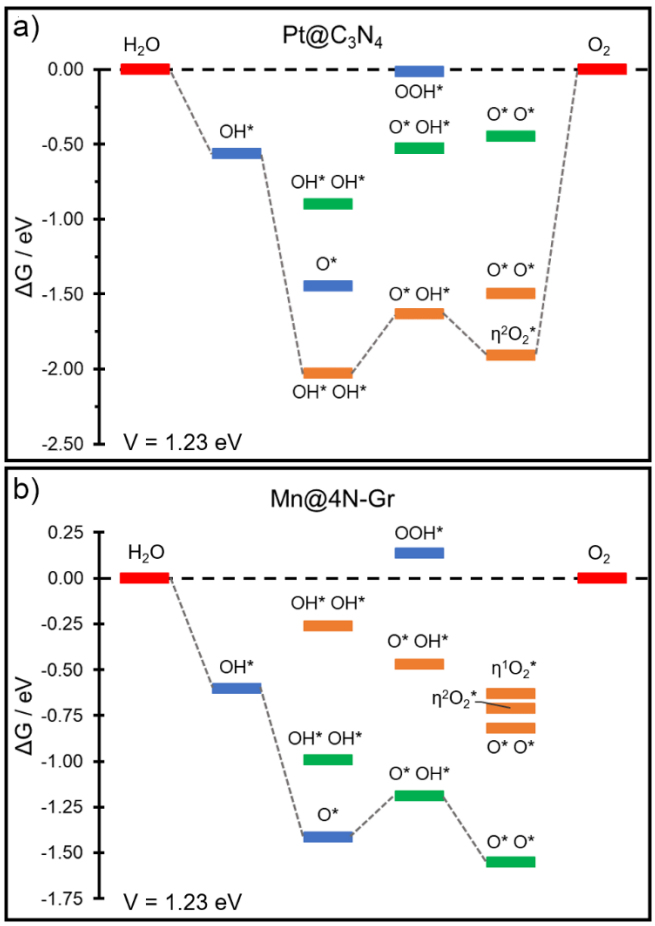

Figure 4: Gibbs energy profile of a) $Pt@C_3N_4$ and b) Mn@4N-Gr. The conventional intermediates are represented in blue, the unconventional *sin* and *anti* are in orange and green, respectively. The Gibbs energy profile is reported at V = 1.23 eV and the experimental reference of O_2 molecule was considered.

5 Conclusions

In this work we simulated a set of 30 Single Atom Catalysts consisting of isolated transition metal atoms stabilized in a carbon matrix with the aim of showing that the Oxygen Evolution Reaction is not likely to occur *via* the classical OH*, O*, and OOH* path. This is the mechanism usually assumed based on the knowledge from extended metal and oxide surfaces.[62] To this end, we adopted a thermodynamic approach where the energies of various intermediates were evaluated at the level of Density Functional Theory. We anchored ten metals (Sc, Ti, V, Cr, Mn, Fe, Co, Ni, Pd and Pt) on three different supports: graphene, nitrogen-doped graphene and carbon nitride. In all cases at least one unconventional chemical intermediate was found to be more stable than the classical one. These are the OH* OH*, OH* O*, O* O*, O_2* complexes. This shows that the assumptions done in

modelling OER on heterogenous catalysts cannot be transferred to the class of SACs without essential modifications.

From the cases discussed, it is apparent that completely different predictions of the activity of SACs in the OER (and of course on the reverse Oxygen Reduction Reaction) can be made if one assumes the formation of the sub-set of classical intermediates only. In fact, the results reported demonstrate that the OER process can follow different paths, with other intermediates besides the classical ones, and that only once all these intermediates are considered and their relative stability has been evaluated on can reliably conclude about the preferred reaction mechanism. Notice that according to a thermodynamic approach the same conclusion holds true for the Oxygen Reduction Reaction (ORR).

Once more, it is important to stress that the scope of this study is not that to predict new potential catalysts for OER based on transition metals stabilized on 2D carbon nanostructures. This is a very important but also very ambitious goal that requires to include all potential terms that contribute to the final reaction energies: solvent effect, role of the applied potential, role of pH (if any), catalyst stability, etc. In our study all these contributions are neglected, which is also the usual approximation done in most of the screening studies of SACs in water splitting.[63,64] Even the role of the exchange-correlation functional must be carefully checked if one is interested in quantitative predictions.[65,66] Recently we have shown how the results can depend on the use of standard GGA functionals or on self-interaction corrected functionals such as hybrid functionals or DFT+*U*.[65] This is true in particular for late transition metal atoms of the 3d series. For all these reasons we do not consider our reported energy profiles of special interest for the design of new catalysts, unless it will be demonstrated that the reaction mechanism remains the same even after all the mentioned effects have been properly included or verified.

The purpose of the study is another one, and in particular it is to alert the computational community toward the need to fully explore the potential energy surface even when relatively simple

reactions such as OER are considered. The present discussion of the OER parallels a recent study from our group where we demonstrated similar effects for the Hydrogen Evolution Reaction (HER).[22] Here dihydrogen or dihydride complexes can form on SACs, at variance with metal electrodes where only isolated H atoms exist before the release of the H_2 molecule. The use of simplified schemes, valid for extended surfaces, does not apply to the case of SACs. This is just another manifestation of the fact that the chemistry of SACs embedded in carbon-based matrices is reminiscent of that of coordination compounds, which is also one reason why SACs are fascinating systems for catalytic reactions.[60,67] The complex and rich chemistry of coordination compounds is more challenging to be modeled, but on the other hand it opens interesting and unexplored opportunities for the design of new systems to be used in heterogenous catalysis.

Another very important message of our paper is that care is needed when large sets of computational data are used to train artificial intelligence algorithms to predict new structures or to extract interaction potentials. Machine learning algorithms interpolate among large amounts of data. If the training set contains only information on a sub-set of possible intermediates, e.g. the OH*, O*, and OOH* intermediates in the OER, the derived interaction potentials will also be affected by this limitation, and may not be able to predict the existence of other intermediates.

In the future we plan to extend this work in three main directions: (1) determine in a systematic way the role of the solvent on the reaction profiles; (2) evaluate the importance of the computational approach and in particular of the exchange-correlation functional on thermochemistry of these processes; and (3) analyze the limiting potentials and the existence (or absence) of scaling relationships and the possible identification of useful descriptors for this class of reactions.

Acknowledgements

We thank Livia Giordano for useful discussions. We acknowledge the financial support from Cariplo foundation. Access to the CINECA supercomputing resources was granted via ISCRAB. We also

thank the COST Action 18234 supported by COST (European Cooperation in Science and Technology).

Author Information

Corresponding Author

Gianfranco Pacchioni, Università Milano-Bicocca, Dipartimento di Scienza dei Materiali, via R. Cozzi 55, 20126 Milano. ORCID: 0000-0002-4749-0751

*E-mail: gianfranco.pacchioni@unimib.it

The manuscript was written through contributions of all authors.

Notes

The authors declare no conflict of interest.

Supporting Information available

Supplementary Tables and Figures are available.

References

[1] M.Z. Rahman, M.G. Kibria, C.B. Mullins, Metal-free photocatalysts for hydrogen evolution, Chem. Soc. Rev. 49 (2020) 1887–1931. https://doi.org/10.1039/C9CS00313D.

[2] J.H. Kim, D. Hansora, P. Sharma, J.-W. Jang, J.S. Lee, Toward practical solar hydrogen production – an artificial photosynthetic leaf-to-farm challenge, Chem. Soc. Rev. 48 (2019) 1908–1971. https://doi.org/10.1039/C8CS00699G.

[3] S. Chen, T. Takata, K. Domen, Particulate photocatalysts for overall water splitting, Nat. Rev. Mater. 2 (2017) 17050. https://doi.org/10.1038/natrevmats.2017.50.

[4] X. Zou, Y. Zhang, Noble metal-free hydrogen evolution catalysts for water splitting, Chem. Soc. Rev. 44 (2015) 5148–5180. https://doi.org/10.1039/c4cs00448e.

[5] D.M. Heard, A.J.J. Lennox, Electrode Materials in Modern Organic Electrochemistry, Angew. Chemie Int. Ed. 59 (2020) 18866–18884. https://doi.org/10.1002/anie.202005745.

[6] B. Qiao, A. Wang, X. Yang, L.F. Allard, Z. Jiang, Y. Cui, J. Liu, J. Li, T. Zhang, Single-atom catalysis of CO oxidation using Pt1/FeOx, Nat. Chem. 3 (2011) 634–641. https://doi.org/10.1038/nchem.1095.

[7] A. Wang, J. Li, T. Zhang, Heterogeneous single-atom catalysis, Nat. Rev. Chem. 2 (2018) 65–81. https://doi.org/10.1038/s41570-018-0010-1.

[8] Y. Tang, C. Asokan, M. Xu, G.W. Graham, X. Pan, P. Christopher, J. Li, P. Sautet, Rh single atoms on TiO2 dynamically respond to reaction conditions by adapting their site, Nat. Commun. 10 (2019) 4488. https://doi.org/10.1038/s41467-019-12461-6.

[9] J.K. Nørskov, J. Rossmeisl, A. Logadottir, L. Lindqvist, J.R. Kitchin, T. Bligaard, H. Jónsson, Origin of the Overpotential for Oxygen Reduction at a Fuel-Cell Cathode, J. Phys. Chem. B. 108 (2004) 17886–17892. https://doi.org/10.1021/jp047349j.

[10] Z.W. Seh, J. Kibsgaard, C.F. Dickens, I. Chorkendorff, J.K. Nørskov, T.F. Jaramillo, Combining theory and experiment in electrocatalysis: Insights into materials design, Science (80-.). 355 (2017) 146. https://doi.org/10.1126/science.aad4998.

[11] I.C. Man, H. Su, F. Calle-Vallejo, H.A. Hansen, J.I. Martínez, N.G. Inoglu, J. Kitchin, T.F. Jaramillo, J.K. Nørskov, J. Rossmeisl, Universality in Oxygen Evolution Electrocatalysis on Oxide Surfaces, ChemCatChem. 3 (2011) 1159–1165. https://doi.org/10.1002/cctc.201000397.

[12] J. Greeley, I.E.L. Stephens, A.S. Bondarenko, T.P. Johansson, H.A. Hansen, T.F. Jaramillo, J. Rossmeisl, I. Chorkendorff, J.K. Nørskov, Alloys of platinum and early transition metals as oxygen reduction electrocatalysts, Nat. Chem. 1 (2009) 552–556. https://doi.org/10.1038/nchem.367.

[13] I.E.L. Stephens, A.S. Bondarenko, F.J. Perez-Alonso, F. Calle-Vallejo, L. Bech, T.P. Johansson, A.K. Jepsen, R. Frydendal, B.P. Knudsen, J. Rossmeisl, I. Chorkendorff, Tuning the Activity of Pt(111) for Oxygen Electroreduction by Subsurface Alloying, J. Am. Chem. Soc. 133 (2011) 5485–5491. https://doi.org/10.1021/ja111690g.

[14] J.K. Nørskov, T. Bligaard, A. Logadottir, J.R. Kitchin, J.G. Chen, S. Pandelov, U. Stimming, Trends in the Exchange Current for Hydrogen Evolution, J. Electrochem. Soc. 152 (2005) J23. https://doi.org/10.1149/1.1856988.

[15] F. Calle-Vallejo, M.D. Pohl, D. Reinisch, D. Loffreda, P. Sautet, A.S. Bandarenka, Why conclusions from platinum model surfaces do not necessarily lead to enhanced nanoparticle catalysts for the oxygen reduction reaction, Chem. Sci. 8 (2017) 2283–2289. https://doi.org/10.1039/C6SC04788B.

[16] N. Govindarajan, M.T.M. Koper, E.J. Meijer, F. Calle-Vallejo, Outlining the Scaling-Based

and Scaling-Free Optimization of Electrocatalysts, ACS Catal. 9 (2019) 4218–4225. https://doi.org/10.1021/acscatal.9b00532.

[17] Á. Valdés, Z.-W. Qu, G.-J. Kroes, J. Rossmeisl, J.K. Nørskov, Oxidation and Photo-Oxidation of Water on TiO 2 Surface, J. Phys. Chem. C. 112 (2008) 9872–9879. https://doi.org/10.1021/jp711929d.

[18] M. Escudero-Escribano, P. Malacrida, M.H. Hansen, U.G. Vej-Hansen, A. Velazquez-Palenzuela, V. Tripkovic, J. Schiotz, J. Rossmeisl, I.E.L. Stephens, I. Chorkendorff, Tuning the activity of Pt alloy electrocatalysts by means of the lanthanide contraction, Science (80-.). 352 (2016) 73–76. https://doi.org/10.1126/science.aad8892.

[19] M.K. Samantaray, V. D'Elia, E. Pump, L. Falivene, M. Harb, S. Ould Chikh, L. Cavallo, J.-M. Basset, The Comparison between Single Atom Catalysis and Surface Organometallic Catalysis, Chem. Rev. 120 (2020) 734–813. https://doi.org/10.1021/acs.chemrev.9b00238.

[20] L. Zhong, S. Li, Unconventional Oxygen Reduction Reaction Mechanism and Scaling Relation on Single-Atom Catalysts, ACS Catal. 10 (2020) 4313–4318. https://doi.org/10.1021/acscatal.0c00815.

[21] J.K. Norskov, C.H. Christensen, Toward Efficient Hydrogen Production at Surfaces, Science (80-.). 312 (2006) 1322 LP – 1323. https://doi.org/10.1126/science.1127180.

[22] G. Di Liberto, L.A. Cipriano, G. Pacchioni, Role of Dihydride and Dihydrogen Complexes in Hydrogen Evolution Reaction on Single-Atom Catalysts, J. Am. Chem. Soc. 143 (2021) 20431–20441. https://doi.org/10.1021/jacs.1c10470.

[23] L.A. Cipriano, G. Di Liberto, G. Pacchioni, Superoxo and Peroxo Complexes on Single Atom Catalysts: Impact on the Oxygen Evolution Reaction, ACS Catal. Just Accep (2022).

[24] N. Vonrüti, R. Rao, L. Giordano, Y. Shao-Horn, U. Aschauer, Implications of Nonelectrochemical Reaction Steps on the Oxygen Evolution Reaction: Oxygen Dimer Formation on Perovskite Oxide and Oxynitride Surfaces, ACS Catal. 12 (2022) 1433–1442. https://doi.org/10.1021/acscatal.1c03308.

[25] J.H. Montoya, A.D. Doyle, J.K. Nørskov, A. Vojvodic, Trends in adsorption of electrocatalytic water splitting intermediates on cubic ABO3 oxides, Phys. Chem. Chem. Phys. 20 (2018) 3813–3818. https://doi.org/10.1039/C7CP06539F.

[26] Y.-L. Lee, M.J. Gadre, Y. Shao-Horn, D. Morgan, Ab initio GGA+U study of oxygen

evolution and oxygen reduction electrocatalysis on the (001) surfaces of lanthanum transition metal perovskites LaBO3 (B = Cr, Mn, Fe, Co and Ni), Phys. Chem. Chem. Phys. 17 (2015) 21643–21663. https://doi.org/10.1039/C5CP02834E.

[27] T. Wang, Y. Zhang, B. Huang, B. Cai, R.R. Rao, L. Giordano, S.-G. Sun, Y. Shao-Horn, Enhancing oxygen reduction electrocatalysis by tuning interfacial hydrogen bonds, Nat. Catal. 4 (2021) 753–762. https://doi.org/10.1038/s41929-021-00668-0.

[28] R.R. Rao, M.J. Kolb, N.B. Halck, A.F. Pedersen, A. Mehta, H. You, K.A. Stoerzinger, Z. Feng, H.A. Hansen, H. Zhou, L. Giordano, J. Rossmeisl, T. Vegge, I. Chorkendorff, I.E.L. Stephens, Y. Shao-Horn, Towards identifying the active sites on RuO2(110) in catalyzing oxygen evolution, Energy Environ. Sci. 10 (2017) 2626–2637. https://doi.org/10.1039/C7EE02307C.

[29] A. Zagalskaya, V. Alexandrov, Role of Defects in the Interplay between Adsorbate Evolving and Lattice Oxygen Mechanisms of the Oxygen Evolution Reaction in RuO2 and IrO2, ACS Catal. 10 (2020) 3650–3657. https://doi.org/10.1021/acscatal.9b05544.

[30] A. Mishra, A. Mehta, S. Basu, N.P. Shetti, K.R. Reddy, T.M. Aminabhavi, Graphitic carbon nitride (g–C3N4)–based metal-free photocatalysts for water splitting: A review, Carbon N. Y. 149 (2019) 693–721. https://doi.org/10.1016/j.carbon.2019.04.104.

[31] Z. Zhao, Y. Sun, F. Dong, Graphitic carbon nitride based nanocomposites: a review, Nanoscale. 7 (2015) 15–37. https://doi.org/10.1039/C4NR03008G.

[32] W.-J. Ong, L.-L. Tan, Y.H. Ng, S.-T. Yong, S.-P. Chai, Graphitic Carbon Nitride (g-C 3 N 4)-Based Photocatalysts for Artificial Photosynthesis and Environmental Remediation: Are We a Step Closer To Achieving Sustainability?, Chem. Rev. 116 (2016) 7159–7329. https://doi.org/10.1021/acs.chemrev.6b00075.

[33] Z. Chen, J. Zhao, C.R. Cabrera, Z. Chen, Computational Screening of Efficient Single-Atom Catalysts Based on Graphitic Carbon Nitride (g-C 3 N 4) for Nitrogen Electroreduction, Small Methods. 3 (2019) 1800368. https://doi.org/10.1002/smtd.201800368.

[34] H. Fei, J. Dong, D. Chen, T. Hu, X. Duan, I. Shakir, Y. Huang, X. Duan, Single atom electrocatalysts supported on graphene or graphene-like carbons, Chem. Soc. Rev. 48 (2019) 5207–5241. https://doi.org/10.1039/C9CS00422J.

[35] H. Fei, J. Dong, M.J. Arellano-Jiménez, G. Ye, N. Dong Kim, E.L.G. Samuel, Z. Peng, Z. Zhu, F. Qin, J. Bao, M.J. Yacaman, P.M. Ajayan, D. Chen, J.M. Tour, Atomic cobalt on

nitrogen-doped graphene for hydrogen generation, Nat. Commun. 6 (2015) 8668. https://doi.org/10.1038/ncomms9668.

[36] K. Liu, S. Kattel, V. Mao, G. Wang, Electrochemical and Computational Study of Oxygen Reduction Reaction on Nonprecious Transition Metal/Nitrogen Doped Carbon Nanofibers in Acid Medium, J. Phys. Chem. C. 120 (2016) 1586–1596. https://doi.org/10.1021/acs.jpcc.5b10334.

[37] Y. Sha, T.H. Yu, B. V. Merinov, P. Shirvanian, W.A. Goddard, Oxygen Hydration Mechanism for the Oxygen Reduction Reaction at Pt and Pd Fuel Cell Catalysts, J. Phys. Chem. Lett. 2 (2011) 572–576. https://doi.org/10.1021/jz101753e.

[38] H.-C. Tsai, T.H. Yu, Y. Sha, B. V. Merinov, P.-W. Wu, S.-Y. Chen, W.A. Goddard, Density Functional Theory Study of Pt 3 M Alloy Surface Segregation with Adsorbed O/OH and Pt 3 Os as Catalysts for Oxygen Reduction Reaction, J. Phys. Chem. C. 118 (2014) 26703–26712. https://doi.org/10.1021/jp507103c.

[39] T. Cheng, W.A. Goddard, Q. An, H. Xiao, B. Merinov, S. Morozov, Mechanism and kinetics of the electrocatalytic reaction responsible for the high cost of hydrogen fuel cells, Phys. Chem. Chem. Phys. 19 (2017) 2666–2673. https://doi.org/10.1039/C6CP08055C.

[40] J.R. Kitchin, Machine learning in catalysis, Nat. Catal. 2018 14. 1 (2018) 230–232. https://doi.org/10.1038/s41929-018-0056-y.

[41] X. Zhang, Z. Zhang, D. Wu, X. Zhang, X. Zhao, Z. Zhou, Computational Screening of 2D Materials and Rational Design of Heterojunctions for Water Splitting Photocatalysts, Small Methods. 2 (2018) 1700359. https://doi.org/10.1002/smtd.201700359.

[42] L. Gong, D. Zhang, C. Lin, Y. Zhu, Y. Shen, J. Zhang, X. Han, L. Zhang, Z. Xia, Catalytic Mechanisms and Design Principles for Single-Atom Catalysts in Highly Efficient CO 2 Conversion, Adv. Energy Mater. 9 (2019) 1902625. https://doi.org/10.1002/aenm.201902625.

[43] F. Calle-Vallejo, R. F. de Morais, F. Illas, D. Loffreda, P. Sautet, Affordable Estimation of Solvation Contributions to the Adsorption Energies of Oxygenates on Metal Nanoparticles, J. Phys. Chem. C. 123 (2019) 5578–5582. https://doi.org/10.1021/acs.jpcc.9b01211.

[44] Z.-D. He, S. Hanselman, Y.-X. Chen, M.T.M. Koper, F. Calle-Vallejo, Importance of Solvation for the Accurate Prediction of Oxygen Reduction Activities of Pt-Based Electrocatalysts, J. Phys. Chem. Lett. 8 (2017) 2243–2246.

https://doi.org/10.1021/acs.jpclett.7b01018.

[45] A. Bouzid, P. Gono, A. Pasquarello, Reaction pathway of oxygen evolution on Pt(1 1 1) revealed through constant Fermi level molecular dynamics, J. Catal. 375 (2019) 135–139. https://doi.org/10.1016/j.jcat.2019.05.025.

[46] Y. Sha, T.H. Yu, Y. Liu, B. V. Merinov, W.A. Goddard, Theoretical Study of Solvent Effects on the Platinum-Catalyzed Oxygen Reduction Reaction, J. Phys. Chem. Lett. 1 (2010) 856–861. https://doi.org/10.1021/jz9003153.

[47] T. Cheng, L. Wang, B. V. Merinov, W.A. Goddard, Explanation of Dramatic pH-Dependence of Hydrogen Binding on Noble Metal Electrode: Greatly Weakened Water Adsorption at High pH, J. Am. Chem. Soc. 140 (2018) 7787–7790. https://doi.org/10.1021/jacs.8b04006.

[48] O. Björneholm, M.H. Hansen, A. Hodgson, L.-M. Liu, D.T. Limmer, A. Michaelides, P. Pedevilla, J. Rossmeisl, H. Shen, G. Tocci, E. Tyrode, M.-M. Walz, J. Werner, H. Bluhm, Water at Interfaces, Chem. Rev. 116 (2016) 7698–7726. https://doi.org/10.1021/acs.chemrev.6b00045.

[49] G. Kresse, J. Hafner, Ab initio molecular dynamics for liquid metals, Phys. Rev. B. 47 (1993) 558–561. https://doi.org/10.1103/PhysRevB.47.558.

[50] G. Kresse, J. Hafner, Ab initio molecular-dynamics simulation of the liquid-metal–amorphous-semiconductor transition in germanium, Phys. Rev. B. 49 (1994) 14251–14269. https://doi.org/10.1103/PhysRevB.49.14251.

[51] G. Kresse, J. Furthmüller, Efficiency of ab-initio total energy calculations for metals and semiconductors using a plane-wave basis set, Comput. Mater. Sci. 6 (1996) 15–50. https://doi.org/https://doi.org/10.1016/0927-0256(96)00008-0.

[52] J.P. Perdew, K. Burke, M. Ernzerhof, Generalized Gradient Approximation Made Simple, Phys. Rev. Lett. 77 (1996) 3865–3868. https://doi.org/10.1103/PhysRevLett.77.3865.

[53] S. Grimme, J. Antony, S. Ehrlich, H. Krieg, A consistent and accurate ab initio parametrization of density functional dispersion correction (DFT-D) for the 94 elements H-Pu, J. Chem. Phys. 132 (2010). https://doi.org/10.1063/1.3382344.

[54] P.E. Blöchl, Projector augmented-wave method, Phys. Rev. B. 50 (1994) 17953–17979. https://doi.org/10.1103/PhysRevB.50.17953.

[55] G. Kresse, D. Joubert, From ultrasoft pseudopotentials to the projector augmented-wave method, Phys. Rev. B. 59 (1999) 1758–1775. https://doi.org/10.1103/PhysRevB.59.1758.

[56] H.J. Monkhorst, J.D. Pack, Special points for Brillouin-zone integrations, Phys. Rev. B. 13 (1976) 5188–5192. https://doi.org/10.1103/PhysRevB.13.5188.

[57] D. Van Dao, L.A. Cipriano, G. Di Liberto, T.T.D. Nguyen, S.-W. Ki, H. Son, G.-C. Kim, K.H. Lee, J.-K. Yang, Y.-T. Yu, G. Pacchioni, I.-H. Lee, Plasmonic Au nanoclusters dispersed in nitrogen-doped graphene as a robust photocatalyst for light-to-hydrogen conversion, J. Mater. Chem. A. 9 (2021) 22810–22819. https://doi.org/10.1039/D1TA05445G.

[58] D. Van Dao, G. Di Liberto, H. Ko, J. Park, W. Wang, D. Shin, H. Son, Q. Van Le, T. Van Nguyen, V. Van Tan, G. Pacchioni, I.-H. Lee, LaFeO 3 meets nitrogen-doped graphene functionalized with ultralow Pt loading in an impactful Z-scheme platform for photocatalytic hydrogen evolution, J. Mater. Chem. A. 10 (2022) 3330–3340. https://doi.org/10.1039/D1TA10376H.

[59] G. Di Liberto, S. Tosoni, G. Pacchioni, Z-Scheme versus type-II junction in g-C 3 N 4 /TiO 2 and g-C 3 N 4 /SrTiO 3 /TiO 2 heterostructures, Catal. Sci. Technol. 11 (2021) 3589–3598. https://doi.org/10.1039/D1CY00451D.

[60] G. Vilé, G. Di Liberto, S. Tosoni, A. Sivo, V. Ruta, M. Nachtegaal, A.H. Clark, S. Agnoli, Y. Zou, A. Savateev, M. Antonietti, G. Pacchioni, Azide-Alkyne Click Chemistry over a Heterogeneous Copper-Based Single-Atom Catalyst, ACS Catal. 12 (2022) 2947–2958. https://doi.org/10.1021/acscatal.1c05610.

[61] J.K. Nørskov, T. Bligaard, J. Rossmeisl, C.H. Christensen, Towards the computational design of solid catalysts, Nat. Chem. 1 (2009) 37–46. https://doi.org/10.1038/nchem.121.

[62] J. Greeley, T.F. Jaramillo, J. Bonde, I. Chorkendorff, J.K. Nørskov, Computational high-throughput screening of electrocatalytic materials for hydrogen evolution, Nat. Mater. 5 (2006) 909–913. https://doi.org/10.1038/nmat1752.

[63] C. Ling, Y. Ouyang, Q. Li, X. Bai, X. Mao, A. Du, J. Wang, A General Two-Step Strategy–Based High-Throughput Screening of Single Atom Catalysts for Nitrogen Fixation, Small Methods. 3 (2019) 1800376. https://doi.org/https://doi.org/10.1002/smtd.201800376.

[64] Z. Chen, J. Zhao, C.R. Cabrera, Z. Chen, Computational Screening of Efficient Single-Atom Catalysts Based on Graphitic Carbon Nitride (g-C3N4) for Nitrogen Electroreduction, Small

Methods. 3 (2019) 1800368. https://doi.org/https://doi.org/10.1002/smtd.201800368.

[65] I. Barlocco, L.A. Cipriano, G. Di Liberto, G. Pacchioni, Modeling Hydrogen and Oxygen Evolution Reactions on Single Atom Catalysts with Density Functional Theory: Role of the Functional, Adv. Theory Simulations. 2200513 (2022) 2200513. https://doi.org/10.1002/adts.202200513.

[66] G. Di Liberto, L.A. Cipriano, G. Pacchioni, Universal Principles for the Rational Design of Single Atom Electrocatalysts? Handle with Care, ACS Catal. 12 (2022) 5846–5856. https://doi.org/10.1021/acscatal.2c01011.

[67] M.A. Bajada, J. Sanjosé-Orduna, G. Di Liberto, S. Tosoni, G. Pacchioni, T. Noël, G. Vilé, Interfacing single-atom catalysis with continuous-flow organic electrosynthesis, Chem. Soc. Rev. 51 (2022) 3898–3925. https://doi.org/10.1039/D2CS00100D.